ACS APPLIED NANO MATERIALS

www.acsanm.org
Article

Europium-Doped Calcium Silicate Nanoparticles as High-Quantum-Yield Red-Emitting Phosphors

Hyun-Joo Woo, Seock-Jin Chung, Meghan L. Hill, Kay Hadrick, and Taeho Kim*

Cite This: ACS Appl. Nano Mater. 2023, 6, 9884−9891
Read Online

ACCESS | Metrics & More | Article Recommendations

ABSTRACT: Europium ion-activated calcium silicate phosphors (Ca_2SiO_4:Eu^{3+}) with sharp red-light emission were fabricated via the hydrothermal method. The size of Ca_2SiO_4:Eu^{3+} phosphors was controlled between 20 and 200 nm by precursor silicate particle sizes. Systematic studies to determine morphology, crystal phase, and photoluminescence (PL) were carried out for all the phosphors, and their optical efficiencies were compared. We found that the luminescence intensity and emission wavelength of Ca_2SiO_4:Eu^{3+} phosphors depend on their particle sizes. Particularly, the Ca_2SiO_4:Eu^{3+} synthesized with 20 nm silica seed contains the most intense red emission, high color purity, and high PL quantum yield. For the 20 nm-sized Ca_2SiO_4:Eu^{3+} phosphor, PL quantum yields are measured to be above 87.95% and high color purity of 99.8%. The unusually high intensity of $^5D_0 \rightarrow {}^7F_4$ emission (712 nm) is explained by structural distortion arising from silicate particle size reductions. We show that the obtained phosphor is a suitable candidate for solid-state lighting as a red component through CIE chromaticity coordinate and color purity measurements. Furthermore, the Ca_2SiO_4:Eu^{3+} particles are examined for their validity as promising bio-imaging probes through cell labeling and imaging experiments and biodegradability studies.

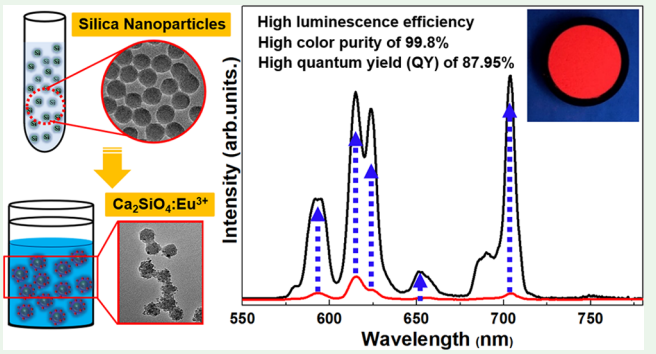

KEYWORDS: *Ca_2SiO_4, silicate, hydrothermal, red fluorescence, quantum yield (QY), biomaterial*

1. INTRODUCTION

For ambient and back lighting in liquid crystal display (LCD), white light emitting diodes (W-LEDs) are widely used because of their high efficiencies.[1−5] Popular W-LEDs are based on a blue LED chip coated with commercial $Y_3Al_5O_{12}$:Ce (YAG:Ce) yellow phosphors.[6−9] However, the commercial W-LEDs have two shortcomings: high correlated color temperature (CCT) and a low color rendering index (CRI). These problems can be overcome by mixing and packaging a high-purity red-emitting and high-quantum efficiency phosphor within the LED.[10−13] Furthermore, in the display industry, mini/micro-LEDs have recently attracted much attention in replacing common LCDs due to their higher energy efficiency, shorter response time, and better contrast. However, to use mini/micro-LEDs as individual pixel elements, it is required to integrate phosphors with small particle sizes, uniform shape/distributions, and size-dependent high internal quantum efficiency.[14−19] Particle size significantly influences the optical properties of phosphorous nanomaterials and thus plays an important role in the packaging performance of phosphor-converted W-LEDs.[20−22]

In this study, we have synthesized calcium silicate using various-sized silica nanoparticle precursors via a hydrothermal method. Dicalcium silicate (Ca_2SiO_4) has many applications as a host material in photoluminescence (PL) due to its affordability, accessibility, chemical stability, thermal resistance, and simple preparation.[23−27] Doping or co-doping of rare-earth ions to the silicate crystal is the prominent strategy for enhancing their luminescence properties.[28−36] Among various rare-earth elements, europium of two valence states (Eu^{3+}, Eu^{2+}) exhibits magnificent luminescence. As most studies use Eu^{2+}-doped Ca_2SiO_4 as bluish-green-emitting phosphors, red-luminescent Ca_2SiO_4:Eu^{3+} phosphors remain understudied.[29,30,32,34] To the best of our knowledge, the luminescence of Eu^{3+}-doped Ca_2SiO_4 red-emitting phosphors has yet to be discussed in detail. Moreover, the optical properties based on particle size dependence of the phosphor have never been studied. These novel probes based on calcium silicate nanoparticles would have promising use within

Received: April 20, 2023
Accepted: May 5, 2023
Published: May 18, 2023

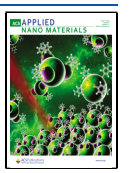

https://doi.org/10.1021/acsanm.3c01547
ACS Appl. Nano Mater. 2023, 6, 9884−9891

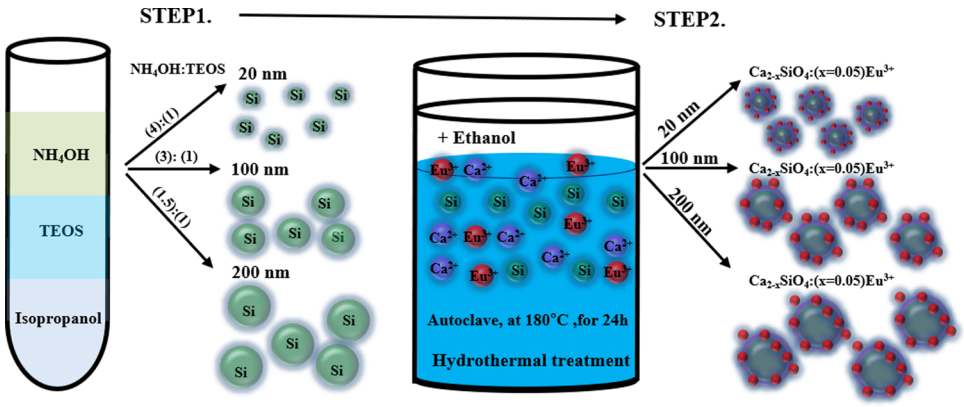

Figure 1. Schematic diagram for the synthesis of trivalent europium ion-doped Ca_2SiO_4 ($Ca_{2-0.05}SiO_4{:}_{0.05}Eu^{3+}$) phosphors.

biological optical imaging due to their high biocompatibility, good bioactivity, and biodegradability.[37−44]

This paper introduces the facile chemical synthesis of the Eu^{3+}-doped Ca_2SiO_4 nanoparticles. It investigates their enhanced optical properties to overcome W-LED disadvantages and presents their potential applications in mini/micro-LEDs and biomaterials.[45] For the first time, we report luminescence properties for the $^5D_0 \rightarrow {}^7F_4$ transition of the Eu^{3+}-doped Ca_2SiO_4 phosphors prepared using various size distributions of silica seed materials (20−200 nm). The prepared 20 nm-sized $Ca_2SiO_4{:}Eu^{3+}$ phosphors exhibited excellent absolute quantum yield and high-purity red emissions. The properties presented here could contribute to highly efficient manufacturing of solid-state lighting devices.[46] For further use in biomaterials, the probes were characterized as efficient imaging markers with enhanced cell uptake and strong red fluorescence.

2. MATERIALS AND METHODS

2.1. Materials. Tetraethyl orthosilicate (TEOS, 99% Cat no. 86578), ammonium hydroxide (NH_4OH, 28−30%, Cat no. A669S-500), Europium(III) nitrate hydrate ($Eu(NO_3)_3{\cdot}5H_2O$, 99%, Cat no. 254061-1G), calcium nitrate tetrahydrate ($Ca(NO_3)_2{\cdot}4H_2O$, 99%, Cat no. 237124-500G), and polyoxyethylene(5) nonylphenylether, branched (IGEPAL@ CO-520, Cat no. 238643-100G), were purchased from Sigma-Aldrich Chemicals (Atlanta, Georgia).

2.2. Synthesis of Silica Nanoparticles (SNPs). SNPs in different sizes were prepared by the in situ silica sol−gel method according to the previous synthetic procedure with some modifications.[46,47] First, IGEPAL was dispersed thoroughly in cyclohexane by sonication for about 10 min and stirred further at 30 °C for 30 min to obtain a homogeneous solution.[48] Next, NH_4OH and TEOS (4:1, 3:1, 1.5:1) were added to the reaction mixture under vigorous stirring overnight at 70 °C to obtain the sphere shape of SNPs. The size of SNPs was controlled by varying ratios of NH_4OH and TEOS (800 μL:200 μL, 600 μL:200 μL, 300 μL:200 μL). Finally, the white precipitate was obtained and then washed three times with deionized water.

2.3. Preparation of Trivalent Europium Ions Doped in Ca_2SiO_4. $Ca_2SiO_4{:}Eu^{3+}$ was prepared through a high-temperature hydrothermal reaction with chemical precursors (or dopants).[49] The above-obtained SNPs were dispersed in ethanol, and the aqueous solution containing the mixture of $Ca(NO_3)_2{\cdot}6H_2O$ and $Eu(NO_3)_3{\cdot}6H_2O$ was added. This mixture was initially stirred at 80 °C for 2 h to get a homogeneous solution. The solution was taken in a 20 mL Teflon-lined autoclave, heated at 180 °C for 24 h to obtain the white precipitates, and then sequentially washed with ethanol and deionized water. Thereafter, it was then subjected to thermal treatment in atmospheric air at 200 °C for 24 h to decompose the organic compound in the sample. Accordingly, a pure white $Ca_{2-0.05}SiO_4{:}_{0.05}Eu^{3+}$ powder was obtained. For comparison, commercial $Ca_{2-0.05}SiO_4{:}_{0.05}Eu^{3+}$ was prepared by the solid-state reaction method by finely grinding conventional SiO_2 (Cat no. S5130, Sigma-Aldrich).[29,30] The obtained products were structurally characterized using a powder X-ray diffractometer (XRD) and transmission electron microscope (TEM). The samples were denoted as C_2S-20, C_2S-100, and C_2S-200 for the prepared probes with the silica precursor of 20, 100, and 200 nm, respectively. It was denoted as C_2S-C for the probe by commercial silica.

2.4. X-ray Diffraction Studies of $Ca_{2-0.05}SiO_4{:}_{0.05}Eu^{3+}$. The host crystal structure of Ca_2SiO_4 was characterized by powder XRD (X'Pert Pro, PANalytical Instrument) operating at 40 kV and 40 mA with Cu Kα radiation (0.154 nm). The XRD analysis was done between the angles (2θ) 10 and 80° with a scan speed of 0.02°/s. The data obtained from the XRD were compared with that from the powder simulation of Inorganic Crystal Structure Database (ICSD) cards.

2.5. Morphological Study of SNPs and $Ca_{2-0.05}SiO_4{:}_{0.05}Eu^{3+}$. The particle size and morphologies of SNPs and $Ca_{2-0.05}SiO_4{:}_{0.05}Eu^{3+}$ nanoparticles were measured using TEM operated at an accelerating voltage of 200 kV (JEOL 2200FS).

2.6. The PL and PL Quantum Yield Studies of $Ca_{2-0.05}SiO_4{:}_{0.05}Eu^{3+}$. The excitation and emission spectra of the $Ca_{2-0.05}SiO_4{:}_{0.05}Eu^{3+}$ nanoparticles were obtained using PL spectroscopy (FP-8500, JASCO, Japan) with a 450 W Xe lamp as the excitation source. The samples were mounted on a polymer stub and were measured for their excitation and emission by maintaining a constant slit width of 0.1 nm for samples.

2.7. CIE. The Commission International de l'Eclairage (CIE) chromaticity coordinates (x, y) were calculated from the obtained emission spectra of the samples by using the CIE calculator. The CCT and color purity were also calculated using the obtained diagram of the CIE chromaticity.

2.8. Biodegradation of $Ca_{2-0.05}SiO_4{:}_{0.05}Eu^{3+}$ Nanoparticles. Biodegradation features of $Ca_{2-0.05}SiO_4{:}_{0.05}Eu^{3+}$ nanoparticles on simulated body fluid (SBF) were characterized by transmission electron microscopy (TEM). The $Ca_{2-0.05}SiO_4{:}_{0.05}Eu^{3+}$ nanoparticles were added to the SBF solution (pH −5). The solution was incubated under stirring slowly at 37 °C for 7 days. The degradation solution was taken out on day 1, day 3, day 5, and day 7 and dropped two to three times on carbon-coated copper grid for TEM analysis.

2.9. Cellular Uptake and Cell Imaging. Four mouse breast cancer T1 cells were incubated in a culture medium with or without nanoparticles for 24 h at 37 °C of the incubator. After incubation, cell uptake of nanoparticles was terminated with three times washes of cold phosphate-buffered saline (PBS), and the cells were collected in 1 mL vial tubes. Cell images were taken by using a UV lamp. The four-T1-cell line was obtained from the American Type Culture Collection (ATCC, Manassas, Virginia). The four T1 cells were grown using Dulbecco's modified Eagle's medium (Sigma-Aldrich Chemicals, Cat no. 11965092) supplemented with 10% fetal bovine

https://doi.org/10.1021/acsanm.3c01547
ACS Appl. Nano Mater. 2023, 6, 9884−9891

serum (Sigma-Aldrich Chemicals, Cat no. 16000044) and 1% penicillin/streptomycin antibiotics (Sigma-Aldrich Chemicals, Cat no. 15070063) in a 37 °C humidified atmosphere containing 5% CO_2.

3. RESULTS AND DISCUSSION

3.1. Synthesis of $Ca_{2-0.05}SiO_4{:}_{0.05}Eu^{3+}$ Nanoparticles. We successfully prepared Eu^{3+}-doped Ca_2SiO_4 ($Ca_{2-0.05}SiO_4{:}_{0.05}Eu^{3+}$) phosphors of various particle sizes through a high-temperature hydrothermal reaction with chemical precursors (or dopants) in the presence of SNP seed. Furthermore, we validated that when we used SNPs of different sizes as seeds, it perfectly controlled the overall particle size of the resulting $Ca_{2-0.05}SiO_4{:}_{0.05}Eu^{3+}$ (Figure 1).

3.2. Effect of Silica Seed Particle Sizes on Structure Properties. The optical nanoparticles with high quantum yield (QY) and sharp PL emission in the red region are necessary for fabricated phosphor-converted LEDs and successful bio-imaging applications. Optical properties such as excitation and emission spectra depend on the crystal structure of nanoparticles. We initially found that the optimal Eu dopant concentration is 5% from previous literatures[29,30] and prepared various-sized $Ca_{2-0.05}SiO_4{:}_{0.05}Eu^{3+}$ nanoparticles (20, 100, 200 nm). The crystal structure has been analyzed to help understand the average crystallite size of the $Ca_{2-0.05}SiO_4{:}_{0.05}Eu^{3+}$ particles by using electron diffraction patterns in TEM and XRD analyses. Particularly, the present study mainly focused on revealing the particle size effects on the crystal structure or luminescence behavior of $Ca_{2-0.05}SiO_4{:}_{0.05}Eu^{3+}$. As shown in the XRD patterns (Figure 2), the $Ca_{2-0.05}SiO_4{:}_{0.05}Eu^{3+}$ samples (C_2S-20, C_2S-100, C_2S-200, C_2S-C) possess the monoclinic crystal structure with the P121/n1 space group, and the lattice parameters are a = 5.51, b = 6.76, and c = 10.4482 A°, α = 90, β = 117.21, and γ = 90. The as-prepared $Ca_{2-0.05}SiO_4{:}_{0.05}Eu^{3+}$ samples showed that the full width at half maximum (FWHM) of the main peak (32.05°) increased with decreased particle sizes. The FWHM can be used to calculate the average crystallite sizes of the particle by using the Scherrer equation ($D_{hkl} = k\lambda/[\beta(2\theta)\cos\theta]$. From the estimated data, we found that the average crystallite sizes of $Ca_{2-0.05}SiO_4{:}_{0.05}Eu^{3+}$ particles (C_2S-20, C_2S-100, C_2S-200, C_2S-C) are 29.21, 32.68, 40.73, and 50.72 nm, respectively. The smaller NP silicate caused a decrease in the crystallite size and enhanced the inter-planar spacing. Also, some lattice distortion was found to be created in the structure of the host material. Furthermore, a slight peak shift toward the higher 2θ diffraction was observed in all the $Ca_{2-0.05}SiO_4{:}_{0.05}Eu^{3+}$ particle samples (C_2S-20, C_2S-100, C_2S-200, C_2S-C). The peak shift in 2θ diffraction is due to the Eu^{3+} dopant insertion to the host, where we speculate the lattice volume compression and lattice constant reduction from Bragg's law.

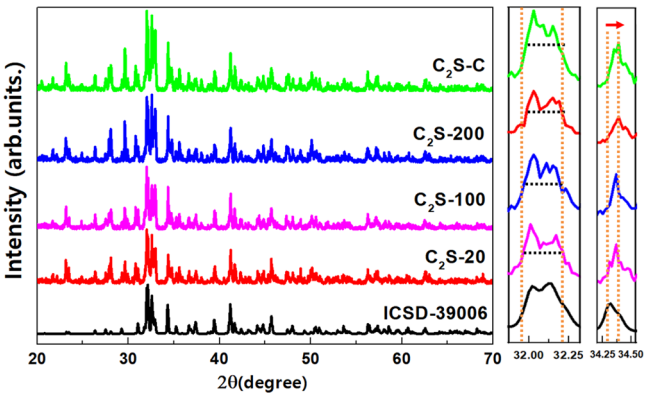

Figure 2. Powder XRD patterns of $Ca_{2-0.05}SiO_4{:}_{0.05}Eu^{3+}$phosphors prepared using conventional SiO_2(C_2S-C) and 20 nm (C_2S-20), 100 nm (C_2S-100), and 200 nm (C_2S-200) silica as silicate sources.

3.3. Structural and Morphological Analyses of $Ca_{2-0.05}SiO_4{:}_{0.05}Eu^{3+}$. The external morphologies of SNPs and $Ca_{2-0.05}SiO_4{:}_{0.05}Eu^{3+}$ were analyzed using TEM and are displayed in Figure 3. The size and morphologies of SNPs were controlled by varying the ratio of TEOS to NH_4OH (NH_4OH:TEOS = 4:1, 2:1, and 1.5:1). The particle size was affected by the amount of NH_4OH that controls the rate of hydrolysis and condensation in the silica sol−gel reaction.[49−53] Figure 3 shows uniform spherical SNPs and their increasing diameter from (a) to (c) with the decreasing NH_4OH amount. Using different sizes of SNPs as silicate sources (seeds), we synthesized the size-controlled $Ca_{2-0.05}SiO_4{:}_{0.05}Eu^{3+}$. Figure 3d−f shows the TEM images depicting all three different sizes of $Ca_{2-0.05}SiO_4{:}_{0.05}Eu^{3+}$ particles. The hydrothermal reaction resulted in uniform $Ca_{2-0.05}SiO_4{:}_{0.05}Eu^{3+}$ with no aggregation. In this two-step procedure, the physical dimension of host materials was regulated by the original silica-seed source; thus, we could fabricate optical $Ca_{2-0.05}SiO_4{:}_{0.05}Eu^{3+}$ nanoparticles with different sizes/morphologies. Interestingly, there is a slight increase in diameter for all particles during the doping procedure of the Ca and Eu ions since the additional graft layers were deposited on the silica host.

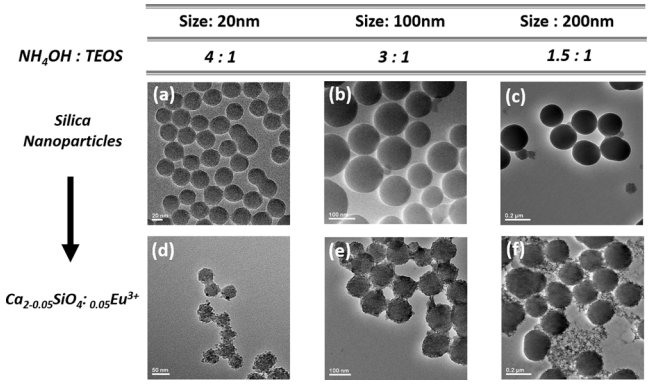

Figure 3. Representative TEM images of various silica particles with sizes of 20 nm (a), 100 nm (b), and 200 nm (c), and TEM images of $Ca_{2-0.05}SiO_4{:}_{0.05}Eu^{3+}$ phosphors C_2S-20 (d), C_2S-100 (e), and C_2S-200 (f) prepared using the silica particles.

3.4. PL Properties of Prepared $Ca_{2-0.05}SiO_4{:}_{0.05}Eu^{3+}$. When measuring the excitation spectra of $Ca_{2-0.05}SiO_4{:}_{0.05}Eu^{3+}$ phosphors at the emission 712 nm maxima, there were major peaks detected at 270 nm and in the range between 300 and 450 nm. The strong excitation from $Ca_{2-0.05}SiO_4{:}_{0.05}Eu^{3+}$ centered at the 270 nm peak is attributed to the charge transfer band (CTB) of Eu^{3+}-O^{2-} because an electron is transferred from the oxygen 2p orbital to the empty 4f orbital of Eu. The excitation efficiency of the CTB was almost the same with $Ca_{2-0.05}SiO_4{:}_{0.05}Eu^{3+}$ phosphors prepared from 100 nm, 200 nm, and commercial silica sources (C_2S-100, C_2S-200, and C_2S-C, respectively). In contrast, the $Ca_{2-0.05}SiO_4{:}_{0.05}Eu^{3+}$ phosphor prepared from 20 nm silica (C_2S-20) has 1.5 times higher excitation efficiency than the other samples. The finding

https://doi.org/10.1021/acsanm.3c01547
ACS Appl. Nano Mater. 2023, 6, 9884−9891

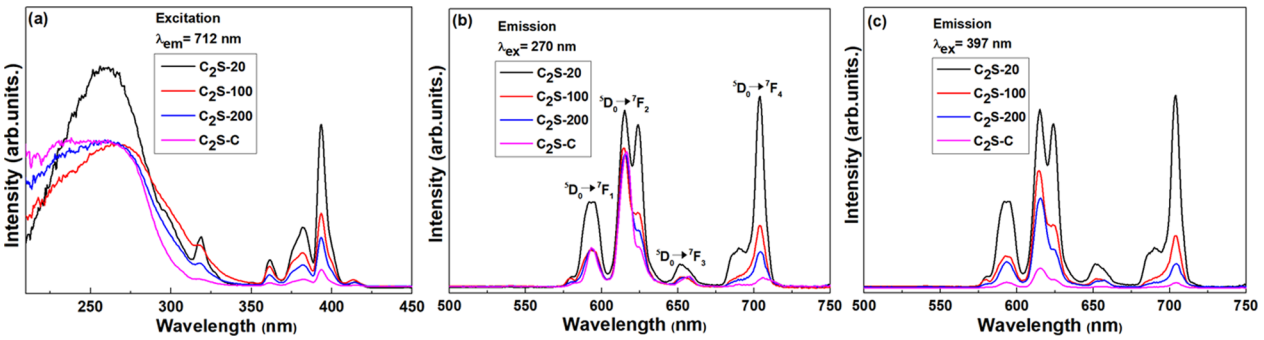

Figure 4. PL excitation at 712 nm (a) and emission spectra excited at 270 nm (b) and 397 nm (c) of the $Ca_{2-0.05}SiO_4{:}_{0.05}Eu^{3+}$ phosphors prepared with various silicate particles (C_2S-20, C_2S-100, C_2S-200, and C_2S-C).

Table 1. Mathematical Value of the Area of the Emission Spectrum and the Height of the Maximum Luminescence Efficiency of Various Silica Particles, Namely, C_2S-20, C_2S-100, C_2S-200, and C_2S-C

	luminescence efficiency (mathematical area/max height)			
	C_2S-20	C_2S-100	C_2S-200	C_2S-C
λ_{ex} = 270 nm wavelength (575−725 nm)	71793.68	37781.46	32923.76	27335.28
λ_{ex} = 270 nm wavelength (712 nm)	22612.45/2064	8105.48/675	5528.50/394	2370.52/116
λ_{ex} = 397 nm wavelength (575−725 nm)	71513.94	31410.31	21870.44	4853.65
λ_{ex} = 397 nm wavelength (712 nm)	22410.45/2061	6691.26/562	3675.86/262	806.37/58

indicates that an efficient energy transfer from the Eu-O CTB to Eu^{3+} occurs on the smaller-sized $Ca_{2-0.05}SiO_4{:}_{0.05}Eu^{3+}$ phosphors (20 nm; C_2S-20). For the excitation spectra between 300 and 400 nm, the intense lines were detected at the $^7F_{0,1}$ ground state to $^5H_{3,6}$ (319 nm), $^5D_4$ (361 nm), $^5L_7$ (381 nm), $^5L_6$ (397 nm), and $^5D_3$ (421 nm) with intra-configurational $^4f_6 \rightarrow {}^4f_6$ transitions of Eu^{3+} ions (Figure 4a). Similar to the excitation maximal at 246 nm for $Ca_{2-0.05}SiO_4{:}_{0.05}Eu^{3+}$ phosphors (20 nm; C_2S-20), the small-sized phosphor samples showed high excitation efficiency at $^7F_0 \rightarrow {}^5L_6$ (397 nm) with the f−f transition of Eu^{3+}. From these findings, we can conclude that the $Ca_{2-0.05}SiO_4{:}_{0.05}Eu^{3+}$ prepared by the 20 nm silica source (C_2S-20) strongly absorbs UV (397 nm), effectively transferring the excitation energy to the photoactive Eu^{3+} ions, presumably showing an efficient emission. From the data, we can speculate that the energy transfer and the resultant excitation efficiency of Eu^{3+} depend on the local environment, in this case the particle size. Next, we conducted the emission spectral measurement for all the $Ca_{2-0.05}SiO_4{:}_{0.05}Eu^{3+}$ samples (C_2S-20, C_2S-100, C_2S-200, C_2S-C) at excitation wavelengths of 246 nm (Figure 4b) and 397 nm (Figure 4c). Although there were no apparent changes in peak position, the peak intensity (luminescent efficiency) for the samples significantly changed by the different transition efficiency of CTB (246 nm) and $^7F_0 \rightarrow {}^5L_6$ (397 nm). It was detected that the luminescence intensity was increased with decreasing particle size. The highest emission intensity was observed for $Ca_{2-0.05}SiO_4{:}_{0.05}Eu^{3+}$ synthesized with 20 nm silica (C_2S-20), and then it decreased sequentially for C_2S-100, C_2S-200, and C_2S-C at both excitations (246 and 397 nm). The emission intensity of the electric dipole transition of $^5D_0 \rightarrow {}^7F_2$ (614 nm) was stronger than the magnetic dipole transitions of $^5D_0 \rightarrow {}^7F_1$ (591 nm) and $^5D_0 \rightarrow {}^7F_0$ (579 nm). Unlike the $^5D_0 \rightarrow {}^7F_1$ (591 nm) transition insensitive to site symmetry and surroundings, the $^5D_0 \rightarrow {}^7F_2$ (614 nm) and $^5D_0 \rightarrow {}^7F_4$ (712 nm) transitions have a hypersensitive electric dipole nature to be affected by the site symmetry. For the $Ca_{2-0.05}SiO_4{:}_{0.05}Eu^{3+}$ samples, when the Eu^{3+} (0.095 nm) ions enter into the host lattice and replace the Ca^{2+}(0.099 nm) ions,[54] vacancies (VCa) are formed owing to the valence differences between Eu^{3+} and Ca^{2+}. Therefore, the site symmetry is reduced and the delocalization of the Eu^{3+} ions occurs in a distorted (or symmetric) cationic environment, which allows the forbidden transition in $Ca_{2-0.05}SiO_4{:}_{0.05}Eu^{3+}$.[55] In particular, there was a considerable increase in emission intensity at the $^5D_0 \rightarrow {}^7F_4$ (712 nm) transition for the 20 nm silicate sample (C_2S-20). There are a few studies for PL properties of the Eu^{3+}-doped Ca_2SiO_4 in the literature;[25,35,56,57] however, those studies were performed to examine how the PL is affected by the adjustment of valence of Eu ions (Eu^{2+}/Eu^{3+}) or host changes. In this study, we focused more on the investigation of structural and spectroscopic changes by the crystal size control of $Ca_2SiO_4{:}Eu^{3+}$. In general, The Judd−Ofelt theory describes a more intense $^5D_0 \rightarrow {}^7F_2$ transition than the $^5D_0 \rightarrow {}^7F_4$ emission due to the optical transition strength parameter Ω4 being much smaller than Ω2. However, as aforementioned, the PL spectra of the Eu^{3+} are inconsistent, especially in the $^5D_0 \rightarrow {}^7F_4$ transition region. Therefore, the $^5D_0 \rightarrow {}^7F_4$ (712 nm) transition was observed to be more dominant than the $^5D_0 \rightarrow {}^7F_2$ transition for the 20 nm silicate sample (C_2S-20), which finally leads to its deep-red phosphor emission with high color saturation. In contrast, the $Ca_{2-0.05}SiO_4{:}_{0.05}Eu^{3+}$ from the 100 nm, 200 nm, and commercial silica sources (C_2S-100, C_2S-200, and C_2S-C, respectively) have shown dominant effects from $^5D_0 \rightarrow {}^7F_2$ transition. Even though the reaction parameters (temperature and Eu^{3+} concentration) used for the particle synthesis were the same in the present study, the f−f transition and the local symmetry properties of Eu^{3+} ions show differently in the $Ca_{2-0.05}SiO_4{:}_{0.05}Eu^{3+}$ phosphors with 20 nm silica sources (C_2S-20). There was no previous study to report our new findings that the values of Ω2 and Ω4 change according to the different sizes of silicate in the sample. Those results confirm that the abnormal $^5D_0 \rightarrow {}^7F_4$ intensity of $Ca_{2-0.05}SiO_4{:}_{0.05}Eu^{3+}$ may be due to the structural distortion arising from the silicate size reduction. References 58−61 suggest an explanation of the

https://doi.org/10.1021/acsanm.3c01547
ACS Appl. Nano Mater. 2023, 6, 9884−9891

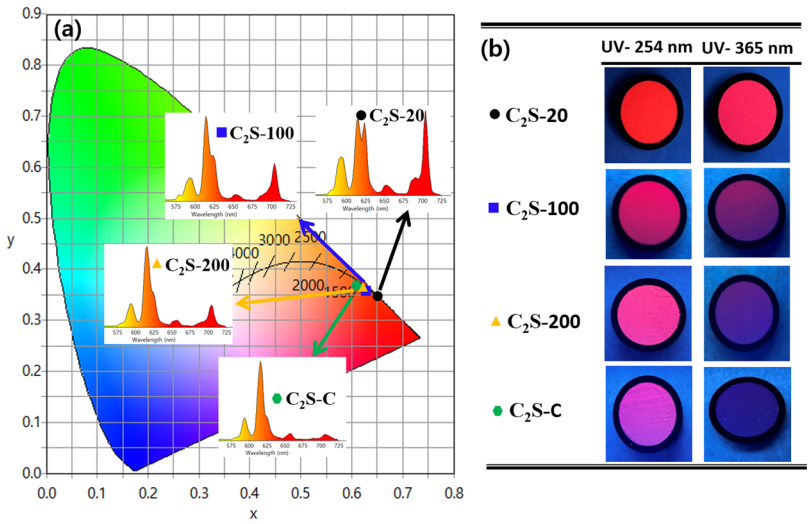

Figure 5. (a) CIE chromaticity coordinates of phosphors for $Ca_{2-0.05}SiO_4{:}_{0.05}Eu^{3+}$, corresponding to the various silicate particles (C_2S-20, C_2S-100, C_2S-200, and C_2S-C). (b)Photographs of these phosphors under UV Lamp (365 nm).

abnormal $^5D_0 \rightarrow {}^7F_4$ intensity based on structural distortion. Chi et al. proposed that the geometry of Eu^{3+}-doped $Ca_2Ga_2GeO_7$ was distorted from cubic to non-cubic.[61,62] They also explain that the geometry distortion of EuO_8 dodecahedron from cubic to square antiprism is responsible for the unusual emission of Eu^{3+}. Based on the information, we could assume that the silicate size strongly affects the f−f transition and the local symmetry properties of Eu^{3+} ions of $Ca_{2-0.05}SiO_4{:}_{0.05}Eu^{3+}$ phosphors. However, there need to be more experimental and theoretical studies to reveal why only 20 nm silicate has super high $^5D_0 \rightarrow {}^7F_4$ intensity for future research.

To investigate the luminescence efficiency, we calculated the value of the area from the emission spectrum and the height of the maximum luminescence efficiency (Table 1). Under maximum excitation at 270 nm (CTB), the $Ca_{2-0.05}SiO_4{:}_{0.05}Eu^{3+}$ sample prepared with a 20 nm silicate source (C_2S-20) increased up to 35% compared to $Ca_{2-0.05}SiO_4{:}_{0.05}Eu^{3+}$ prepared with commercial silica (C_2S-C) in the entire emission spectrum (575−725 nm). As a result, the efficiency of the $^5D_0 \rightarrow {}^7F_4$ transition was about 130%, and when the maximum emission height was compared at 712 nm, the efficiency improved by more than 200%. When comparing the emission intensity upon the excitation of the $^7F_0 \rightarrow {}^5L_6$ (397 nm) transition, the emission efficiency from 575 to 725 nm increased by 130%. Furthermore, the efficiency and maximum intensity heights of the $^5D_0 \rightarrow {}^7F_4$ (712 nm) transition also increased by 270 and 400%, respectively.[63,64] The PL QY is a critical parameter to evaluate the performance of the phosphor material. The quantum yields of $Ca_{2-0.05}SiO_4{:}_{0.05}Eu^{3+}$ at the excitation wavelength of 397 nm were calculated for the samples made of 20 nm = 87.95%, 100 nm = 22.11%, 200 nm = 20.84%, and commercial silica = 6.51%. Notably, PL quantum yields for $Ca_{2-0.05}SiO_4{:}_{0.05}Eu^{3+}$ with 20 nm silicate are measured to be above 87.95%, superior to that of available rare earth oxide salt phosphors, and the value is even higher than commercial rare earth nitride red phosphors.[65−67]

3.5. CIE. The color coordinates are a critical parameter for evaluating the performance of photoluminescence materials. The CIE chromaticity coordinates were determined from the emission spectra of the samples. As shown in Figure 5a, CIE chromaticity coordinate values of $Ca_{2-0.05}SiO_4{:}_{0.05}Eu^{3+}$ prepared with various silicate seed sizes can be observed: C_2S-20 = (x:0.670, y:0.351), C_2S-100 = (x:0.637, y:0.359), C_2S-200 = (x:0.633, y:0.363), and C_2S-C = (x:0.633, y:0.362). The $Ca_{2-0.05}SiO_4{:}_{0.05}Eu^{3+}$ phosphors have the color coordinates shifted toward the deep red region with decreasing silicate size. Therefore, the $Ca_{2-0.05}SiO_4{:}_{0.05}Eu^{3+}$ synthesized with 20 nm silica seed had a closer value to the commercial red-emitting phosphors (e.g., $Y_2O_3{:}Eu^{3+}$ (0.65, 0.35), $Y_2O_2S{:}Eu^{3+}$ (0.622, 0.351)) and the standard of the National Television System Committee (NTSC) (0.67, 0.33). These results indicate that decreasing the particle sizes of silicate improves the red color purity. Next, we calculated the color purity of the samples using the obtained CIE coordinate (x, y) data. The resulting color purities of the $Ca_{2-0.05}SiO_4{:}_{0.05}Eu^{3+}$ synthesized with 20 nm, 100 nm, 200 nm, and commercial silicate are as high as 99.8, 99.2, 99.1, and 98.9%, respectively. In addition, the color purity was cross-validated with the luminescence photographs of samples. Although all the samples showed red fluorescence emission,[68−70] only the 20 nm-sized $Ca_{2-0.05}SiO_4{:}_{0.05}Eu^{3+}$ revealed the most prominent deep red emission under UV lamp irradiation (365 and 254 nm) (Figure 5b). Conclusively, the $Ca_{2-0.05}SiO_4{:}_{0.05}Eu^{3+}$ synthesized with 20 nm silica contains intense red emission, very high color purity, and excellent optical property, which indicates that the obtained phosphor is a potential candidate for solid-state lighting as a red component.

3.6. Biodegradability and Cell Imaging. Ideal biomaterials should have high biocompatibility and good biodegradability to ensure high biosafety. Calcium silicate, a candidate host material to anchor fluorescent dyes or dope luminescent rare-earth ions for bio-imaging, is well known for its excellent biodegradability.[41−44] Interestingly, the lattice defects caused by ion doping can accelerate the degradation of the silicate materials and small-sized nanoparticles are more easily degraded due to a higher surface area to volume ratio (S/V ratio) and more increased surface energies than those of large-sized counterparts. Therefore, we expected $Ca_{2-0.05}SiO_4{:}_{0.05}Eu^{3+}$ nanoparticles to have attractive degradation potentials in biological media. We incubated our nanoparticles in SBF at 37 °C and examined the color change of particle suspension upon overtime degradation. TEM

https://doi.org/10.1021/acsanm.3c01547
ACS Appl. Nano Mater. 2023, 6, 9884−9891

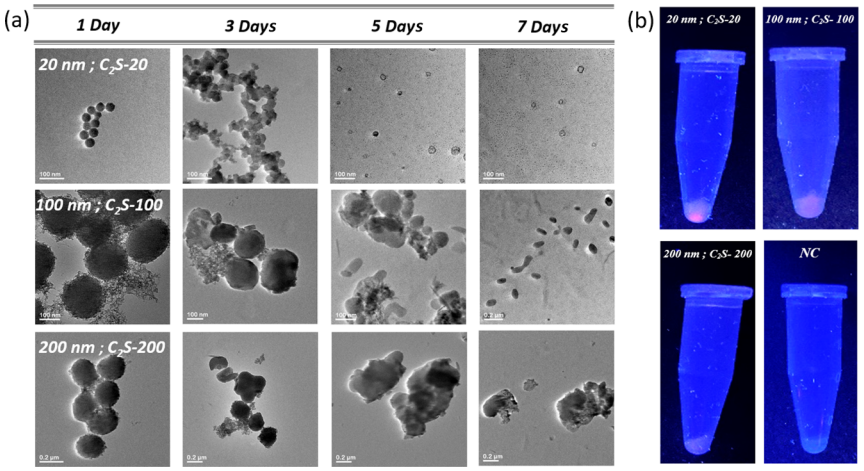

Figure 6. (a) TEM images showing the morphology changes of $Ca_{2-0.05}SiO_4{:}_{0.05}Eu^{3+}$ nanoparticles (20, 100, 200 nm) after incubation with SBF. Scale bars = 200 nm. (b) Fluorescence images of the pelleted cells labeled with $Ca_{2-0.05}SiO_4{:}_{0.05}Eu^{3+}$ (20, 100, 200 nm particles, and PBS) under UV lamp (365 nm).

images show that our particles noticeably deteriorated in a week with structural damage (Figure 6a). 20 nm-sized particles (C_2S-20) showed the highest degradation rate among all specimens, and silicate nanoparticles were mostly degraded in 7 days. Figure 6b shows the fluorescence imaging capability of the particles after labeling them to cells. For the experiments, the nanoparticles (10 mg) were incubated in four T1 cells for 24 h at 37 °C. We confirmed that the fluorescence signals were shown in four T1 cells using a UV lamp after the 24 h nanoparticle treatment. The 20 nm nanoparticle-treated cells have shown the highest fluorescence signals among the three different size particle-treated cells. The 20 nm particles (C_2S-20), which retain enhanced particle-to-cell interactions and better colloidal stability than the large counterparts (100 nm, C_2S-100; 200 nm, C_2S-200), might contribute to the bright fluorescence signals. However, the governing factor for the prominent fluorescence imaging signatures from the cell pellets is primarily due to the intensive red emission from the 20 nm-sized $Ca_{2-0.05}SiO_4{:}_{0.05}Eu^{3+}$ nanoparticles (C_2S-20). Taken together, the 20 nm-sized $Ca_{2-0.05}SiO_4{:}_{0.05}Eu^{3+}$ nanoparticles (C_2S-20) have shown their potential as efficient fluorescence imaging probes.

4. CONCLUSIONS

In summary, we have successfully fabricated size-controlled, $Ca_{2-0.05}SiO_4{:}_{0.05}Eu^{3+}$ phosphors by using precursor silica seeds with different particle sizes. The emission intensity of the phosphors is inversely proportional to the particle sizes, with the highest intensity with a 20 nm-sized phosphor (C_2S-20). The emission intensity of the C_2S-20 phosphor increased four times (400%) compared to the C_2S-C phosphor. The C_2S-20 phosphors show strong intensity due to the $^5D_0 \rightarrow {}^7F_4$ transition of Eu^{3+}, possibly due to the structural distortion arising from the silicate size reduction. The PL QY of the C_2S-20 phosphor was measured to be 87.95%. Moreover, the C_2S-20 phosphors showed a high color purity of 99.8% with CIE chromaticity coordinates of (x:0.670, y:0.351). The $Ca_{2-0.05}SiO_4{:}_{0.05}Eu^{3+}$ synthesized with 20 nm silica seed contains intense red emission, high color purity, high quantum yield, good optical properties, and great potential for red luminescent materials in solid-state lighting devices. Additional cell imaging experiments show their promise as bio-imaging probes. Overall, these results show that the small-sized $Ca_{2-0.05}SiO_4{:}_{0.05}Eu^{3+}$ (20 nm; C_2S-20) can be a promising red phosphor for WLEDs, for mini/micro-LEDs, or in biomaterial applications.

AUTHOR INFORMATION

Corresponding Author

Taeho Kim − *Department of Biomedical Engineering, Institute for Quantitative Health Science and Engineering, Michigan State University, East Lansing, Michigan 48824, United States;* orcid.org/0000-0002-7500-8918; Email: kimtae47@msu.edu

Authors

Hyun-Joo Woo − *Department of Biomedical Engineering, Institute for Quantitative Health Science and Engineering, Michigan State University, East Lansing, Michigan 48824, United States*

Seock-Jin Chung − *Department of Biomedical Engineering, Institute for Quantitative Health Science and Engineering, Michigan State University, East Lansing, Michigan 48824, United States*

Meghan L. Hill − *Department of Biomedical Engineering, Institute for Quantitative Health Science and Engineering, Michigan State University, East Lansing, Michigan 48824, United States*

Kay Hadrick − *Department of Biomedical Engineering, Institute for Quantitative Health Science and Engineering, Michigan State University, East Lansing, Michigan 48824, United States*

Complete contact information is available at: https://pubs.acs.org/10.1021/acsanm.3c01547

Notes

The authors declare no competing financial interest.

ACKNOWLEDGMENTS

T.K. acknowledges fund support from Michigan State University (Departmental Start-Up Grant) and the National Institutes of Health (R01HD108895).

REFERENCES

(1) Ye, S.; Xiao, F.; Pan, Y. X.; Ma, Y. Y.; Zhang, Q. Y. Phosphors in phosphor-converted white light-emitting diodes: Recent advances in materials, techniques and properties. *Mater. Sci. Eng. R.* **2010**, *71*, 1−34.

(2) Liu, Q.; Wang, L.; Huang, W.; Li, X.; Yu, M.; Zhang, Q. Thermally stable double perovskite $CaLaMgSbO_6:Eu^{3+}$ phosphors as a tunable LED-phosphor material. *Ceram. Int.* **2018**, *44*, 1662−1667.

(3) Huang, A.; Yang, Z.; Yu, C.; Chi, Z.; Qiu, J.; Song, Z. Tunable and White Light Emission of a Single-Phased $Ba_2Y(BO_3)_2Cl:Bi^{3+},Eu^{3+}$ Phosphor by Energy Transfer for Ultraviolet Converted White LEDs. *J. Phys. Chem. C* **2017**, *121*, 5267−5276.

(4) Fukuda, Y.; Sato, T. White-Light-Emitting Diodes Using Sr-Containing Sialon Phosphors. *Jpn. J. Appl. Phys.* **2012**, *51*, 122103−122104.

(5) NaKamura, S.; Fasol, G. *The Blue Laser Diode* (Springer-Verlag: Berlin). 1977, P.216.

(6) Feng, H.; Yang, Y.; Zhang, X. G.; Xu, Y.; Guan, J. Synthesis and luminescence of Sr2SiO4:Eu3+ micro-sperical phosphor by a spray-drying process. *Superlattices Microstruct.* **2015**, *78*, 150−155.

(7) Nakamura, S.; Mukai, T.; Senoh, M. Candela-class high-brightness InGaN/AlGaN double-heterostructure blue-light-emitting diodes. *Appl. Phys. Lett.* **1994**, *64*, 1687−1689.

(8) Zhao, Y.; Xu, H.; Zhang, X.; Zhu, G.; Yan, D.; Yu, A. Facile synthesis of $YAG:Ce^{3+}$ thick films for phosphor converted white light emitting diodes. *J. Eur. Ceram. Soc.* **2015**, *35*, 3761−3764.

(9) Zhang, Y.; Luo, L.; Chen, G.; Liu, Y.; Liu, R.; Chen, X. Green and red phosphor for LED backlight in wide color gamut LCD. *J. Rare Earths* **2020**, *38*, 1−12.

(10) Zhang, N.; Wang, D.; Li, L.; Meng, Y.; Zhang, X.; Ming, N. YAG:Ce Phosphors for WLED via nano-pseudoboehmite sol−gel route. *J. Rare Earths* **2006**, *24*, 294−297.

(11) Schlotter, P.; Baur, J.; Hielscher, C.; Kunzer, M.; Obloh, H.; Schmidt, R.; Schneider, J. Fabrication and characterization of GaN/InGaN/AlGaN double heterostructure LEDs and Their application in luminescence conversion LEDs. *Mat. Sci. Eng.B.* **1999**, *59*, 390−394.

(12) Wang, B.; Lin, H.; Xu, J.; Chen, H.; Wang, Y. $CaMg_2Al_{16}O_{27}:Mn^{4+}$-based red phosphor: A potential color converter for high-powered warm W-LED. *ACS Appl. Mater. Interfaces* **2014**, *6*, 22905−22913.

(13) Cao, R.; Zhang, F.; Cao, C.; Yu, X.; Liang, A.; Guo, S.; Xue, H. Synthesis and luminescence properties of $CaAl_2O_4:Mn^{4+}$ phosphor. *Opt. Mater.* **2014**, *38*, 53−56.

(14) Chen, H.; Ju, L.; Zhang, L.; Wang, X.; Zhang, L.; Xu, X.; Gao, L.; Qui, K.; Yin, L. Exploring a particle-size-reduction strategy of YAG:Ce phosphor via a chemical breakdown method. *J. Rare Earths* **2021**, *39*, 938−945.

(15) Gou, F.; Hsiang, E.-L.; Tan, G.; Lan, Y.-F.; Tsai, C.-Y.; Wu, S.-T. High performance color-converted micro-LED displays. *J. Soc. Inf. Disp.* **2019**, *27*, 199−206.

(16) Tian, P.; McKendry, J. J.; Gong, Z.; Zhang, S.; Waston, S.; Zhu, D.; Watson, I. M.; Gu, E.; Kelly, A. E.; Humphreys, C. J.; Dawson, M. D. Characteristics and applications of Micro-pixelated GaN-based light emitting diodes on Si substrates. *J. Appl. Phys.* **2014**, *115*, 033112−033116.

(17) Huang, Y.; Tan, G.; Gou, F.; Guo, F. W.; Li, M. C.; Lee, S. L.; Wu, S. T. Prospects and challenges of mini-LED and micro-LED displays. *J. Soc. Inf. Disp.* **2019**, *27*, 387−401.

(18) Ahn, H. A.; Hong, S. K.; Kwon, O. K. An active matrix micro-pixelated LED display driver for high luminance uniformity using resistance mismatch compensation method. IEEE Trans. Circuits Syst. II Exp. *Briefs.* **2018**, *65*, 724−728.

(19) Wu, T.; Sher, C. W.; Lin, Y.; Lee, C. F.; Liang, S. J.; Lu, Y. J.; Chen, S. W. H.; Guo, W. J.; Kuo, H. C.; Chen, Z. Mini-LED and Micro-LED: promising candidates for the next generation display technology. *Appl. Sci.* **2018**, *8*, 1557−1517.

(20) Wang, W. N.; Widiyastuti, W.; Ogi, T.; Lenggoroe, W. Correlations between crystallite/particle size and photo-luminescence properties of submicrometer phosphors. *Chem. Mater.* **2007**, *19*, 1723−1730.

(21) Hua, Y. J.; Ma, H. P.; Zhang, C.; Deng, D. G.; Zhao, S. L.; Huang, L. H.; Wang, H. P.; Xu, S. Q. Synthesis and packaging performance of regular spherical $YAG:Ce^{3+}$ phosphors for white LEDs. *Chin J Lumin.* **2013**, *34*, 427−432.

(22) Lee, S. H.; Kang, T. W.; Kim, J. S. The Size Effect and Its Optical Simulation of $Y_3Al_5O_{12}:Ce^{3+}$ Phosphors for White LED. *J. Semicond Disp. Technol.* **2019**, *18*, 10−13.

(23) Sato, Y.; Kato, H.; Kobayashi, M.; Masaki, T.; Yoon, D. H.; Kakihana, M. Tailoring of deep-red luminescence in $Ca_2SiO_4:Eu^{2+}$. *Angew. Chem., Int. Ed.* **2014**, *53*, 7756−7759.

(24) Zhang, Y.; Chen, J.; Li, Y.; Seo, H. J. Monitoring of hydroxyapatite conversion by luminescence intensity of Eu^{3+} ions during mineralization of Eu^{3+}-doped β-Ca_2SiO_4. *Opt. Mater.* **2014**, *37*, 525−530.

(25) Wei, F.; Jia, Q. Massive production of $A_2SiO_4:Eu^{3+}$ and $A_2SiO_4:Eu^{2+}$ (A = Ca, Sr, Ba) microspheres and luminescent properties. *Superlattices Microstruct.* **2015**, *82*, 11−17.

(26) Nakano, H.; Yokoyama, N.; Banno, H.; Fukuda, K. Enhancement of PL intensity and formation of core-shell structure in annealed $Ca_{2-x/2}(Si_{1-x}P_x)O_4:Eu^{2+}$ phosphor. *Mater. Res. Bull.* **2016**, *83*, 502−506.

(27) Wang, Q.; Li, F.; Shen, X.; Shi, W.; Li, X.; Guo, Y.; Xiong, S.; Zhu, Q. Relation Between Reactivity and Electronic Structure for α'L-, β- and γ-Dicalcium Silicate: A First-Principles Study. *Cem. Concr. Res.* **2014**, *57*, 28−32.

(28) Lu, X. L.; Wang, S. X.; Liu, S. X.; Du, P.; Ye, Z. M.; Geng, X. F.; Cheng, X. Phase Identification of γ- and β-Ca_2SiO_4 via the Rear-Earth Fluorescence Probe. *J. Phys. Chem. C* **2019**, *123*, 13877−13884.

(29) Mayavan, A.; Ganesamurthi, J. S.; Jang, K. W.; Gandhi, S. Development of bluish green-emitting $Ca_{2-x}Eu_xSiO_4$ phosphor: A novel approach using silica nanoparticles as precursor. *J. Luminescense* **2021**, *203*, 117664−117669.

(30) Woo, H. J.; Gandhi, S.; Shin, D. S.; Lee, H. S.; Jayasimhadri, M.; Jang, K. W. Engendering color tunable emission in calcium silicate based via ageing of silicate source. *Sens. Actuators, B* **2017**, *241*, 1106−1110.

(31) Woo, H. J.; Kim, T. H. Self-activated rare earth free phosphor prepared by propylene glycol-modified silane. *Result in Chem.* **2023**, *5*, 100824−100827.

(32) Jang, H. S.; Kim, H. Y.; Kim, Y. S.; Lee, H. M.; Jeon, D. Y. Yellow-emitting γ-$Ca_2SiO_4:Ce^{3+}$, Li^+ phosphor for solid-state lighting: luminescent properties, electronic structure, and white light-emitting diode application. *Opt. Express* **2012**, *20*, 2761−2771.

(33) Lou, Y. Y.; Jo, D. S.; Senthil, K.; TeZuka, S.; Kakihana, M.; Toda, K.; Masaki, T.; Yoon, D. H. Synthesis of high efficient $Ca_2SiO_4:Eu^{2+}$ green emitting phosphor by a liquid phase precursor method. *J. Solid State Chem.* **2012**, *189*, 68−74.

(34) Kalaji, A.; Mikami, M.; Cheetham, A. K. Ce^{3+}-Activated γ-Ca_2SiO_4 and other olivine-type ABXO4 phosphors for solid-state lighting. *Chem. Mater.* **2014**, *26*, 3966−3975.

(35) Mani, R.; Jiang, H.; Gupta, S. K.; Li, Z.; Duan, X. Role of synthesis method on luminescence properties of europium(II, III) ions in β-Ca_2SiO_4:probing local site and structure. *Inorg. Chem.* **2018**, *57*, 935−950.

(36) Nakano, H.; Ando, S.; Kamimoto, K.; Hiramatsu, Y.; Michiue, Y.; Hirosaki, N.; Fukuda, K. Incommensurately Modulated Crystal Structure and Photoluminescence Properties of Eu_2O_3- and P_2O_5-Doped Ca_2SiO_4 Phosphor. *Materials* **2020**, *13*, 58.

(37) Zhu, Y. J.; Guo, X. X.; Sham, T. K. Calcium silicate-based drug delivery systems. *Expert Opinion on Drug Delivery* **2017**, *14*, 215−228.

(38) Wu, C.; Chang, J.; Fan, W. Bioactive mesoporous calcium−silicate nanoparticles with excellent mineralization ability, osteostimulation, drug-delivery and antibacterial properties for filling apex roots of teeth. *J. Mater. Chem.* **2012**, *22*, 16801−16809.

(39) Wu, J.; Zhu, Y. J.; Cao, S. W.; Chen, F. Hierachically nanostructured mesoporous spheres of calcium silicate hydrate:

https://doi.org/10.1021/acsanm.3c01547
ACS Appl. Nano Mater. 2023, 6, 9884−9891

surfactant-free sonochemical synthesis and drug-delivery system with ultrahigh drug-loading capacity. *Adv. Mater.* **2010**, *22*, 749−753.
(40) Wu, J.; Zhu, Y. J.; Chen, F.; Zhao, X. Y.; Zhao, J.; Qi, C. Amorphous calcium silicate hydrate/block copolymer hybrid nanoparticles: synthesis and application as drug carriers. *Dalton Trans.* **2013**, *42*, 7032−7040.
(41) Cai, A. Y.; Zhu, Y. J.; Qi, C. Biodegradable Inorganic Nanostructured Biomaterials for Drug Delivery. *Adv. Mater. Interfaces* **2020**, *7*, 2000819.
(42) Gou, Z.; Chang, J.; Zhai, W.; Wang, J. Study on the self-setting property and the in vitro bioactivity of beta-Ca_2SiO_4. *J. Biomed. Mater. Res. Part B.* **2005**, *73*, 244−251.
(43) Mazón, P.; De Aza, P. N. Porous scaffold prepared from α'L-Dicalcium silicate doped with phosphorus for bone grafts. *Ceram. Int.* **2018**, *44*, 1856−1861.
(44) Wang, F.; Xu, Z.; Zhang, Y.; Li, J.; Nian, S.; Zhou, N. Green synthesis and bioactivity of vaterite-doped beta-dicalcium silicate bone cement. *Ceram. Int.* **2016**, *42*, 1856−1861.
(45) Panigrahi, K.; Nag, A. Challenges and Strategies to Design Phosphors for Future White Light Emitting Diodes. *J. Phys. Chem. C* **2022**, *126*, 8553−8564.
(46) Md Nanfiujjaman, M.; Chung, S. J.; Kalashnikova, I.; Hill, M. L.; Homa, S.; George, J.; Contag, C. H.; Kim, T. H. Biodegradable Hollow Manganese Silicate Nanocomposites to Alleviate Tumor Hypoxia toward Enhanced Photodynamic Therapy. *ACS Appl. Bio Mater.* **2020**, *3*, 7989−7999.
(47) Kim, T. H.; Monin, E.; Choi, J. H.; Yuan, K.; Zaidi, H.; Kim, J. Y.; Park, M. H.; Lee, N. H.; McMahon, M. T.; Quinones-Hinojosa, A.; Bulte, J. W. M.; Hyeon, T. G.; Gilad, A. A. Mesoporous Silica Coated Hollow Manganese Oxide Nanoparticles as T_1 Contrast Agent for Labeling and MRI Tracking of Adipose Derived Mesenchymal Stem Cells. *J. Am. Chem. Soc.* **2011**, *133*, 2955−2961.
(48) Darr, J. A.; Zhang, J.; Makwana, N. M.; Weng, X. Continuous Hydrothermal Synthesis of Inorganic Nanoparticles: Applications and Future Directions. *Chem. Rev.* **2017**, *117*, 11125−11238.
(49) Klabunde, K. J.; Stark, J.; Koper, O.; Mohs, C.; Park, D. G.; Decker, S.; Jiang, Y.; Lagadic, L.; Zhang, D. Nanocrystals as Stoichiometric Reagents with Unique Surface Chemistry. *J. Phys. Chem.* **1996**, *100*, 12142−12153.
(50) Hench, L. L.; West, J. K. The Sol-Gel process. *Chem. Rev.* **1990**, *90*, 33−72.
(51) Hormo, E. U.; Kyriazi, M. E.; Kanaras, A. G. A method for the growth of uniform silica shells on different size and morphology upconversion nanoparticles. *Nanoscale Adv.* **2021**, *3*, 3522−3529.
(52) Meyns, M.; Perélvarez, M.; Heuer-Jungemann, A.; Hertog, W.; Ibanez, M.; Nafraia, R.; Genc, A.; Arbiol, J.; Kovalenko, M. V.; Carreras, J.; Cabot, A.; Kanaras, A. G. Polymer-Enhanced Stability of Inorganic Perovskite Nanocrystals and Their Application in Color Conversion LEDs. *ACS Appl. Mater. Interfaces* **2016**, *30*, 19579−19586.
(53) Baker, C. R.; Lewns, F. K.; Poologasundarampillai, G.; Ward, A. D. In Situ Sol-Gel Synthesis of Unique Silica Structures Using Airborne Assembly: Implications for In-Air Reactive Manufacturing. *ACS Appl. Nano Mater.* **2022**, *5*, 11699−11706.
(54) Kim, D. H.; Pi, J. W.; Jung, G. W.; Kim, J. S.; Park, K. Photoluminescence Optimization of $Ca_3(PO_4)_2$:Eu^{3+} Phosphors By Crystallinity Improvement And Charge Compensation. *Res. Square* **2021**, *25*, 1−25.
(55) Wen, J.; Yeung, Y.; Ning, L.; Duan, C.; Huang, Y.; Zhang, J.; Yin, M. Effects of Vacancies on Valence Stabilities of Europium Ions in β-Ca_2SiO_4:Eu Phosphors. *J. Lumin.* **2016**, *178*, 121−127.
(56) Baran, A.; Barzowska, J.; Grinberg, M.; Mahlik, S.; Szczodrowski, K.; Zorenko, Y. Binding energies of Eu^{2+} and Eu^{3+} ions in β-Ca_2SiO_4 doped with europium. *Opt. Mat.* **2013**, *35*, 2107−2114.
(57) Ozturk, E.; Karacaoglu, E.; Durdak, S. Luminescence Properties of Ca_2SiO_4:Eu^{3+} and Zn_2SiO_4:Eu^{3+}. *AKADEMIK PLATFORM.* **2015**, 2404−2410.
(58) Lu, X.; Wang, S.; Liu, S.; Du, P.; Ye, P.; Ye, Z.; Geng, X.; Cheng, X. Pase Identification of γ- and β-Ca_2SiO_4 via the Rear-Earth Fluorescence Probe. *J. Phys. Chem. C* **2019**, *123*, 13877−13884.
(59) Bettinelli, M.; Speghini, A.; Piccinelli, A. N. C.; Malta, O. L. Luminescence spectroscopy of Eu^{3+} in $Ca_3Sc_2Si_3O_{12}$. *J. Lumin.* **2011**, *131*, 1026−1028.
(60) Li, Y.; Li, N.; Zhang, P.; Wei, Z.; Wang, Z.; Zhao, L.; Chen, W. Deep-red photoluminescence from enhanced $^5D_0$-$^7F_4$ transition in Eu^{3+} doped $Ca_2Ga_2GeO_7$ phosphors. *Spectrochim. Acta, Part A* **2021**, *248*, No. 119247.
(61) Chen, D.; Miao, S.; Liang, Y.; Wang, W.; Yan, S.; Bi, J.; Sun, K. Controlled synthesis and photoluminescence properties of Bi_2SiO_5:Eu^{3+} core-shell nanospheres with an intense $^5D_0 \rightarrow {}^7F_4$ transition. *Opt. Mater. Exp.* **2021**, *11*, 355−370.
(62) Chi, F.; Wei, X.; Zhou, S.; Chen, Y.; Duan, C.; Yin, M. Enhanced $^5D_0 \rightarrow {}^7F_4$ transition and optical thermometry of garnet type $Ca_3Ga_2Ge_3O_{12}$:Eu^{3+} phosphors. *Inorg. Chem. Front.* **2018**, *5*, 1288−1293.
(63) Li, B.; Liu, M.; Shi, X.; Cao, Q.; Ni, Z.; Lu, C.; Pan, D. Room-Temperature and Ultrafast Synthesis of Highly Luminescent and Extremely Small Eu^{3+}-Doped YVO_4 Nanocrystals. *J. Phys. Chem. C* **2023**, *127*, 5075−5081.
(64) Gao, P.; Li, Q.; Li, S.; Gai, S.; Li, Y.; Ma, Y.; Zhang, Z.; Molokeev, M. S.; Zhou, Z.; Xia, M. Multiple Strategies to Approach High-Efficiency Luminescence Controllable in Blue/Cyan/Green-Emitting Bi^{3+} -Activated phosphors. *J. Phys. Chem. C* **2022**, *126*, 9195−9206.
(65) Zhu, H.; Lin, C.; Luo, W.; Shu, S.; Liu, Z.; Liu, Y.; Kong, E.; Cao, Y.; Liu, R.; Chen, X. Highly efficient non-rare-earth red emitting phosphor for warm white light-emitting diodes. *Nat. Commun.* **2014**, *5*, 4312.
(66) Ye, W.; Zhao, C.; Shen, X.; Ma, C.; Deng, Z.; Li, Y.; Wang, Y.; Zuo, C.; Wen, Z.; Li, Y.; Li, Y.; Yuan, X.; Wang, C.; Zuo, C.; Yingkui, L.; Yuan, X.; Wang, C.; Cao, W. High Quantum Yield $Gd_{4.67}Si_3O_{13}$:Eu^{3+} Red-Emitting Phosphor for Tunable White Light-Emitting Devices Driven by UV or Blue LED. *ACS Appl. Electron. Mater.* **2021**, *3*, 1403−1412.
(67) Wu, M.; Chen, B.; He, C.; Huang, X.; Liu, Q.; Min, X.; Mi, R.; Wu, X.; Fang, M.; Liu, Y.; Huang, Z. A high quantum yield red phosphor $NaGdSiO_4$:Eu^{3+} with intense emissions from $^5D_0 \rightarrow {}^7F_{1,2}$ transition. *Ceram. Int.* **2022**, *48*, 23213−23223.
(68) Gao, X.; Song, F.; Khan, A.; Chen, Z.; Ju, D.; Sang, X.; Feng, M.; Liu, L. Room temperature synthesis, Judd Ofelt analysis and photoluminescence properties of down-conversion $K_{0.3}Bi_{0.7}F_{2.4}$:Eu^{3+} orange red phosphors. *J. Lumin.* **2021**, *230*, No. 117707.
(69) Pradhan, P.; Singh, K.; Maram, P. S.; Vaidyanathan, S. Oxide-Based Red Emitting Phosphors with High Color purity and Their Vesatile Applications: Synthesis, Structure, and Luminescence properties. *ACS Appl. Opt. Mater.* **2023**, *1*, 132−146.
(70) Hou, J.; Yin, W.; Dong, L.; Li, Y.; Liu, Y.; Liu, Z.; Zhao, G.; Zhang, G.; Fang, Y. A Novel Red-Emitting Na_2NbOF_5:Mn^{4+} Phosphor with Ultrahigh Color Purity for Warm White Lighting and Wide-Gamut Backlight Displays. *Materials.* **2021**, *14*, 5317.

https://doi.org/10.1021/acsanm.3c01547
ACS Appl. Nano Mater. 2023, 6, 9884−9891